JOURNAL OF PROPULSION AND POWER
Vol. 19, No. 3, May–June 2003

Optimization of Electric Thrusters for Primary Propulsion Based on the Rocket Equation

Monika Auweter-Kurtz* and Helmut Kurtz†
Universität Stuttgart, 70550 Stuttgart, Germany

During the last decade, electric propulsion systems have been established for orbit maintenance of satellites. More than 150 spacecraft are now equipped with almost 400 thrusters for this purpose. The current decade will see the use of electric propulsion for primary propulsion. Optimal mission parameters are determined for these tasks. Depending on the mission profile, ion thrusters, Hall thrusters, thermal arcjets, or magnetoplasmadynamics (MPD) thrusters are preferable. All electric propulsion systems have in common that they can be operated over a wide range of specific impulse and that the thrust efficiency and, therefore, the specific power of the propulsion system depend strongly on the specific impulse. The optimal specific impulse for a particular mission depends, therefore, on the kind of thruster and the chosen propellant. It is demonstrated that for MPD, ion, Hall ion, and thermal arcjet thrusters the optimal specific impulse for a particular mission can be determined by an optimization that is based on the rocket equation. In addition, when a simple cost function is used, the influence of the cost factors is explained. Finally, the results of a few missions for which electric propulsion systems have been selected as primary propulsion are discussed.

Nomenclature

a	=	parameter, m/s
b	=	parameter, s/m
c_e	=	effective exhaust velocity, m/s
E	=	specific energy, J/kg
e	=	elementary charge, C
f, f_1	=	functions
g	=	function
$g_{I,II}$	=	examples of function g
k	=	factor
m_{LS}	=	payload and structure mass, kg
m_P	=	propellant mass for achieving mission, kg
m_{PS}	=	propulsion system dry mass (including power supply), kg
m_0	=	initial vehicle mass, kg
$\dot{m}$	=	propellant flow rate, kg/s
P_{el}	=	electrical power, W
T	=	thrust, N
TR	=	transport rate, s^{-1}
v_A	=	Alfvèn velocity, m/s
α_F	=	specific power of propulsion system, W/kg
α_{PS}	=	specific power of power supply, W/kg
Δv	=	velocity increment for mission, m/s
η_{PC}	=	efficiency of power conditioner
η_T	=	thrust efficiency
$\eta_{T,\max}$	=	maximum (theoretical) thrust efficiency
μ_{LS}	=	payload and structure mass fraction
τ	=	trip time, s
$\tau^*_{I,II}$	=	normalized trip time

Received 16 November 2001; revision received 9 September 2002; accepted for publication 7 January 2003.

*Professor, Institut für Raumfahrtsysteme, Pfaffenwaldring 31; auweter@irs.uni-stuttgart.de.

†Aerospace Engineer, Institut für Raumfahrtsysteme, Pfaffenwaldring 31; kurtz@irs.uni-stuttgart.de.

Introduction

TODAY there is no question that electric propulsion systems are serious competitors for primary propulsion with respect to orbit transfer, lunar, or interplanetary missions. Depending on the mission profile, different electric thruster types [thermal arcjets, magnetoplasmadynamics (MPD), ion, and Hall ion thrusters] are either being discussed, have been investigated or developed, or have even been space-proofed for these purposes.[1–5]

Since the early 1970s, the advantages and disadvantages of electric propulsion vs chemical propulsion for transfer missions have been discussed in many papers,[6,7] as well as the comparison between the different types of electric thrusters.[7–11] In general, only the rocket equation in these papers is varied and applied to different thruster types and different mass distributions, without special regard to optimization.

All of the thruster types taken into consideration have in common that the effective exhaust velocity can vary greatly, whereby the thruster efficiency also changes. In this paper, for each thruster type and appropriate propellant, the optimal effective exhaust velocity for a certain velocity increment of the mission will be ascertained. The flight time at a maximum payload capacity should be as low as possible. In the older, valuable works of Langmuir,[12] Irving,[13] and Stuhlinger,[14] and in a U.S. Air Force study,[15] such optimizations have already been made, although under the assumption of a constant specific power α_F of the propulsion system. However, the specific power

$$\alpha_F = \eta_{\mathrm{PC}} \eta_T(c_e)\, \alpha_{\mathrm{PS}} \tag{1}$$

depends on the efficiency of the power conditioning unit η_{PC}, the specific power of the power system α_{PS}, and the thruster efficiency η_T. The specific power α_{PS} is defined as the ratio of electrical power and the sum of power supply mass, power conditioner mass, and motor mass. Whereas the efficiency η_{PC} and the specific power of the system α_{PS} can be seen as independent of the specific impulse as long as the motor mass is much lower than the power supply mass, this is not the case for the thruster efficiency η_T. For all of the electrical thrusters considered here, the thruster efficiency, and, therefore, α_F, strongly depends on the effective exhaust velocity c_e. Therefore, it is absolutely necessary to introduce this dependency into the rocket equation for optimization purposes. This has already been done and published in a previous paper,[16] and it was shown that the Langmuir[12]–Irving[13] optimization is a borderline case.

Because the costs of orbital mass transfer are not only determined by the amount of payload but also by the transfer time, a transport

rate has been defined and is included in the optimization. Especially for crewed missions, the trip time should be minimized not only because of cost but also for safety reasons. In a previous paper,[16] a method was provided for a quick evaluation of the optimal range of the thruster parameters for a certain mission profile for ion and MPD thrusters. During the last 10 years, Hall ion thrusters and thermal arcjets have also shown performance data that make them interesting candidates as primary propulsion systems.[4,17] Therefore, in this paper it is shown that the methods that have already been developed for ion and MPD thrusters can also be applied for Hall ion thrusters and high-power thermal arcjets. For three examples of recent missions, Deep Space 1,[1] SMART-1,[2] and MUSES-C,[3] the predicted optimal effective exhaust velocity is compared to the values for which the selected thrusters have been qualified. A new method for thermal arcjet thrusters is also introduced.

Optimization Based on the Rocket Equation

For the evaluation of a thruster system, the attainable velocity increment is of great interest. The connection between the attainable velocity increment Δv, the required flight time τ, the payload and structure fraction μ_{LS}, on the one hand, and the propulsion system characterized by the effective exhaust velocity c_e and specific power α_F, on the other hand, is provided by the rocket equation. For rockets with energy sources separate from the propellant, that is, mainly electrical thrusters, it can be written in dimensionless form:

$$\frac{\Delta v}{c_e} = \ln\left[\frac{1 + c_e^2/2\alpha_F\tau}{\mu_{LS} + c_e^2/2\alpha_F\tau}\right] \tag{2}$$

where $\sqrt{(2\alpha_F\tau)}$ is a characteristic velocity, which can be derived from the specific energy ε of the propulsion system, $\varepsilon = \alpha_F\tau$ (Ref. 18). The payload and structure mass fraction is defined as $\mu_{LS} = m_{LS}/m_0$, with m_0 as initial mass of the spacecraft and m_{LS} as sum of the payload and structure mass. To compare electric propulsion systems with chemical rockets, the total mass is divided as

$$m_0 = m_{LS} + m_{PS} + m_P \tag{3}$$

with the propellant mass m_P and the mass of the propulsion system including the power system m_{PS}. The propulsion system has to be optimized so that a maximum payload mass fraction μ_{LS}, a minimum flight time τ, and a maximum velocity increment Δv can be achieved. To obtain the conditions for these requirements, the rocket equation (2) is solved for μ_{LS}, τ, and Δv, respectively, and partial differentiation is taken with respect to the exhaust velocity c_e. An investigation of the second derivative reveals that, as required, a maximum and a minimum are being dealt with. When the rocket equation (2) is substituted into all three obtained equations, they can be brought into the same form.[16] This signifies that the minimal flight time, maximal payload fraction, and maximal velocity increment yield one and the same condition and are, therefore, reached at the same time. Furthermore, in this condition, the term dependent on the specific power α_F can be separated, that is, it can be represented in the form $g = f$, where g is a function only of α_F and c_e, whereas f is a function only of μ_{LS} and $\Delta v/c_e$:

$$\underbrace{\frac{c_e}{\alpha_F}\frac{\partial\alpha_F}{\partial c_e}}_{g} = \underbrace{2 + \frac{\Delta v}{c_e}\exp\left(\frac{\Delta v}{c_e}\right)\frac{\mu_{LS} - 1}{[1 - \exp(\Delta v/c_e)][\mu_{LS}\exp(\Delta v/c_e) - 1]}}_{f} \tag{4}$$

The function f, which is independent of the propulsion parameter α_F, can be displayed with $\Delta v/c_e$ as an abscissa and with the payload and structure fraction μ_{LS} as a parameter, which is done in Fig. 1. From Fig. 1, it can be clearly seen that there is no optimization possible for f and g values between 1 and 2, respectively. For further discussion, the function g, which is a function of the specific power of the propulsion system, has to be derived. The specific power α_F strongly depends on the thruster type and propellant choice.

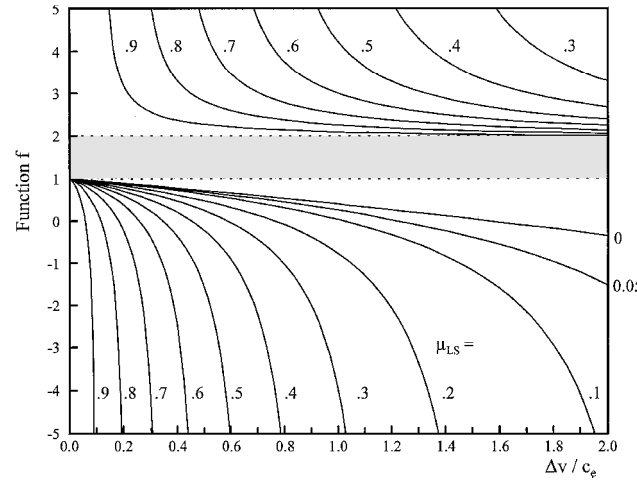

Fig. 1 Function f vs $\Delta v/c_e$ with the payload plus structure mass fraction μ_{LS} as parameter.

High-Power Thermal Arcjets, Ion, Hall Ion, and MPD Thrusters

For ion, Hall ion, and MPD thrusters, as well as for high-power thermal arcjets, the degree of ionization is close to one or at least constant over a wide range of operation. Consequently, the reaction losses of the beam do not significantly change. On the other hand, the thermal losses in these thrusters are low compared to the thrust power and to the other losses and/or do not significantly change. Therefore, the thrust efficiency η_T defined as thrust power divided by total power input can be approximated by the formula

$$\eta_T = \eta_{T,\max}\left\{c_e^2/\left[c_e^2 + (kv_A)^2\right]\right\} \tag{5}$$

already used by Stuhlinger for ion thrusters.[14] Here, $\eta_{T,\max}$ is an asymptotic value for $c_e \to \infty$, which includes, primarily, the thermal and the nozzle losses. The second factor on the right-hand side of Eq. (5) represents the quotient of the kinetic energy of the beam divided by its enthalpy. The velocity v_A is the Alfvèn critical velocity, that is, the average velocity a particle would reach in the case that the sum of the reaction energy, heat of fusion, and heat of evaporation were changed into kinetic energy:

$$v_A = \sqrt{\frac{2e}{\bar{m}_A}\left(\alpha_D E_D + \sum_i \alpha_{I,i} E_{I,i}\right) + 2r_F + r_E} \tag{6}$$

with $\bar{m}_A$ the average atomic mass, α_D the degree of dissociation, $\alpha_{I,i}$ the degree of ionization of the grade, E_D (in electron volts) the dissociation energy, $E_{I,i}$ (in electron volts) the averaged ionization energy of the ith grade, r_F (in joules per kilogram) the specific heat of fusion, and r_E (in joules per kilogram) the specific heat of vaporization. In Table 1, the Alfvén critical velocities for various propellants for full ionization (only first stage) are listed.

In Fig. 2, it is clearly visible that the Alfvén critical velocity strongly depends on the average atomic mass and on its location within the periodic table of elements as found by Bühler.[19] Low values are achievable for high atomic masses and for alkali metals. For ion and Hall ion thrusters, the atomic weight of the propellant should be as high as possible to achieve a high-thrust level. In this case, as can be seen from Fig. 2, the Alfvén critical velocity is also lowest, which means the thrust efficiency, or at least $\eta_{T,\max}$, is high. In the case of MPD thrusters, the propellant selection is not dominated by the request to achieve a high-thrust level but by the demand to increase the effective exhaust velocity and improve the thruster efficiency. To achieve high specific impulses, the average atomic

Table 1 Molecular weights, ionization E_I and dissociation energies E_D, heat of fusion r_F, heat of vaporization r_E, and Alfvén velocity v_A (for complete first ionization) for the most important propellants

	Molecular mass							
Propellant	Cold	Fully dissociated	E_D, eV	$E_{I,1}$, eV	$E_{I,2}$, eV	r_F, J/kg	r_E, J/kg	v_A, km/s
Hydrogen, H_2	2	1	2.26	13.59	——	5.78×10^4	4.60×10^5	55.1
Methane, CH_4	16	3.2	3.45	13.12	——	5.86×10^4	5.48×10^5	31.5
Helium, He	4	4	——	24.48	54.4	——	2.09×10^4	34.24
Ammonia, NH_3	17	4.25	3.04	13.83	——	3.39×10^5	1.37×10^6	27.63
Hydrazine, N_2H_4	32	5.33	3.06	13.9	——	3.96×10^5	1.28×10^6	24.75
Water, H_2O	18	6	3.2	13.6	——	3.34×10^5	2.26×10^6	23.28
Lithium, Li	6.94	6.94	——	5.39	75.62	6.64×10^5	2.13×10^7	13.76
Nitrogen, N_2	28.02	14.01	4.92	14.53	29.59	2.57×10^4	1.99×10^5	16.32
Oxygen, O_2	32	16	2.58	13.61	35.11	1.38×10^4	2.13×10^5	19.69
Sodium, Na	23	23	——	5.14	47.29	1.13×10^5	5.86×10^6	7.00
Potassium, K	39.1	39.1	——	4.34	31.81	5.96×10^4	2.29×10^6	4.87
Argon, Ar	39.95	39.95	——	15.76	27.62	3.03×10^4	1.57×10^5	8.72
Xenon, Xe	131.3	131.3	——	12.13	21.2	2.34×10^4	9.63×10^4	4.24
Cesium, Cs	132.91	132.91	——	3.89	25.1	1.55×10^4	5.02×10^5	2.58
Mercury, Hg	200.59	200.59	——	10.43	18.75	1.17×10^4	3.01×10^5	3.25

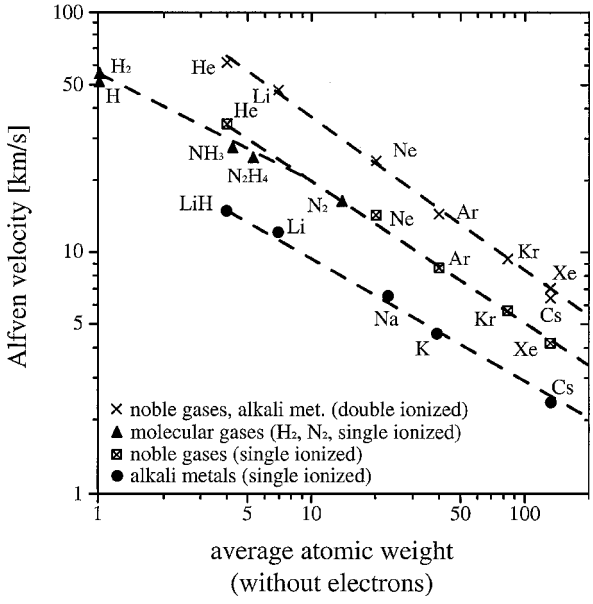

Fig. 2 Alfvèn velocity as function of the average atomic weight (without electrons).

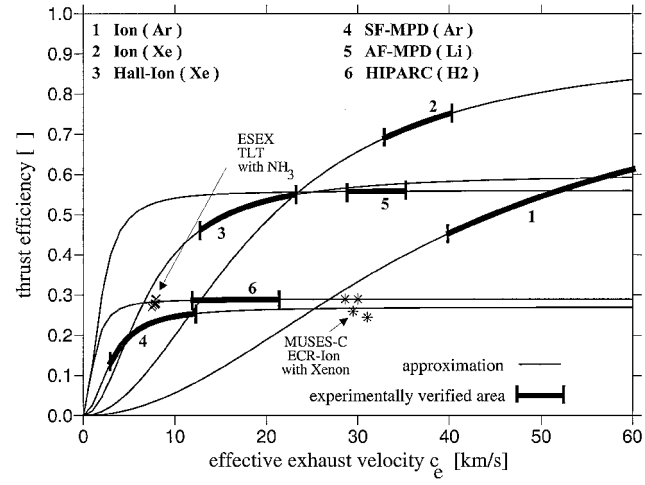

Fig. 3 Thruster efficiency vs effective exhaust velocity for different thrusters (Table 2).

weight of the propellant should be low with respect to the thermal thrust portion. The magnetic thrust portion does not depend on the propellant choice. For self-field MPD thrusters, it can be shown[18] that the effective exhaust velocity c_e is restricted to the Alfvén velocity, if the thermal thrust portion is low compared to the MPD thrust. Both imply the choice of a lightweight propellant. On the other hand, to improve the magnetic thrust, the current I has to be as high as possible because the magnetic thrust is proportional to I^2. This means that the power has to be supplied at a low voltage. Therefore, propellants with low arc voltage levels are preferable. To achieve high efficiencies, the Alfvén velocity should be low. When all of these arguments are taken into account, argon and alkali metals are a good choice for MPD devices. Whether, for example, hydrogen is of interest depends mainly on the magnitude of the thermal thrust fraction. For thermal arcjets, the atomic mass of the propellant should be as low as possible to achieve the highest specific impulses possible.[18] To maximize efficiency, the current level of operation should be minimized because the anode loss, which is dominant for these devices, increases linearly with the current. When all of these points are taken into consideration, hydrogen, which offers a high-voltage level, is the best propellant choice for thermal arcjets, although its Alfvén velocity is the highest.

The factor k in the Eq. (5) makes it possible to consider the average losses that occur during the production of an ion in a certain thruster. Therefore, the term kv_A can be described as an effective "thruster specific" Alfvén velocity. A propulsion system consisting of a certain thruster and propellant is, therefore, characterized by $\eta_{T,\max}$ and kv_A. Approximation (5) corresponds quite well to the measured efficiencies of plasma and ion engines.

In Fig. 3, some experimental results of MPD, ion, high-power thermal arcjet, and Hall ion engines approximated with Eq. (5) are plotted (Table 2). In Fig. 3, the experimentally verified areas are shown with a thick line. By the introduction of Eq. (5) into the left-hand side of Eq. (4), the function $g_I(kv_A, c_e)$ results, which is valid for ion, Hall ion, and MPD thrusters and high-power thermal arcjets as a special case of $g(\alpha_F, c_e)$:

$$g_I = 2\Big/\left[1 + (c_e/kv_A)^2\right] = 2\Big/\left[1 + (c_e/\Delta v)^2(\Delta v/kv_A)^2\right] \quad (7)$$

When plotted against $\Delta v/c_e$ with the thruster type and mission-dependent parameter $kv_A/\Delta v$, one obtains the set of curves displayed together with the function f in the upper part of Fig. 4.

The solutions for an optimized thruster are the points $f = g_I$. Because of the limitations of g_I, $0 \le g_I \le 2$, and the lack of f values in the region $1 < f < 2$, the optimization is limited to $0 < f, g_I < 1$. Furthermore, from Fig. 4, it is obvious that in general $\Delta v/c_e$ is also restricted, and with increasing $kv_A/\Delta v$, the area of $\Delta v/c_e$, in which an optimization is possible, gets smaller. Another important result can be derived: With the increasing sensitivity of $\eta_T(c_e)$, to rising $kv_A/\Delta v$ for a given mission, the optimal specific impulses become greater. The corresponding flight time of a mission can be achieved by introducing Eq. (5) into the optimization condition (4) and using

Table 2 Different thruster types and propellants [with approximation (5)]

Thruster	Propellant	kv_a, km/s	v_a, km/s	k	$\eta_{\tau,\max}$	c_e area experimentally verified, km/s	Ref.
Ion	Ar	36.99	8.72	4.242	0.84	40–60	20
Ion	Xe	19.67	4.24	4.639	0.93	30–40	20
SPT	Xe	7.01	4.24	1.653	0.6	13–23	21
SF-MPD	Ar	3.06	8.72	0.351	0.27	3–11	5
AF-MPD	Li	1.88	13.76	0.137	0.56	29–35	22, 23
HIPARC	H_2	1.199	55.1	0.022	0.29	12–21	4

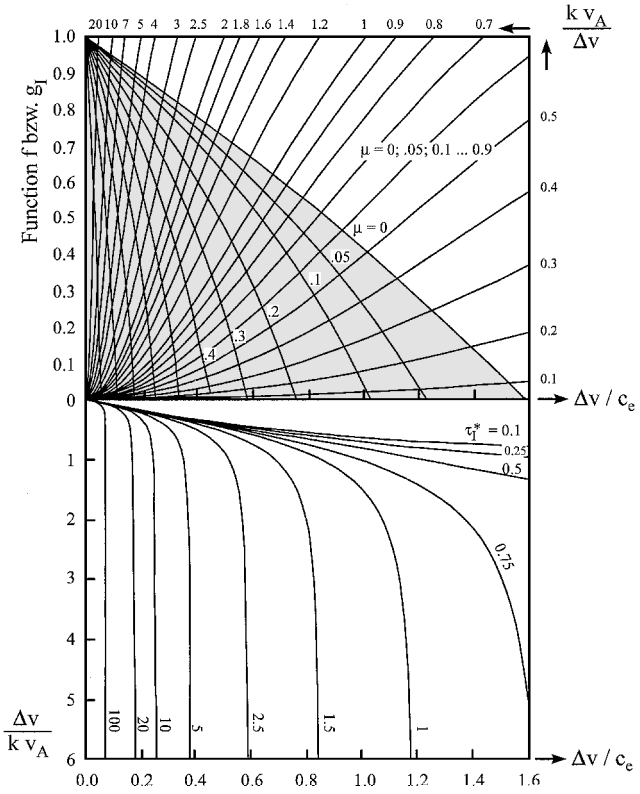

Fig. 4 Nomograph of the quantities Δv, τ_I^*, μ_{LS}, and c_e for the optimized rocket equation for high-power thermal arcjets, ion, Hall ion and MPD thrusters.

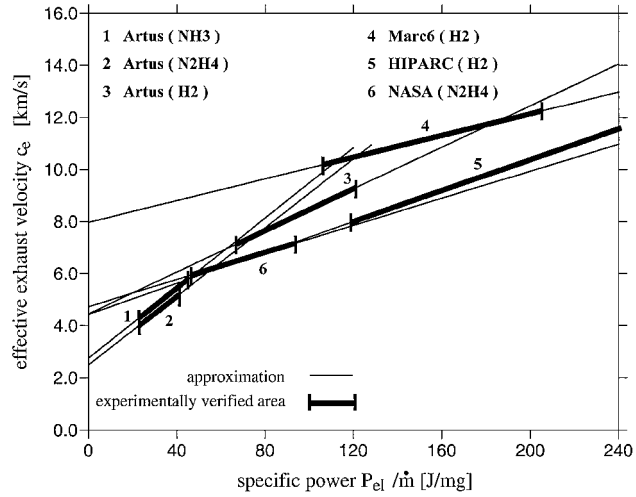

Fig. 5 Effective exhaust velocity c_e as function of specific power for different thermal arcjet thrusters and propellants (Table 3).

the rocket equation (2) for eliminating the payload and structure mass fraction. When a normalized flight time is introduced,

$$\tau_I^* = \eta_{\mathrm{PC}}\alpha_{\mathrm{PS}}\eta_{T,\max}(\tau/\Delta v^2) \tag{8}$$

we achieve

$$\tau_I^* = \left\{\frac{c_e}{\Delta v}\left[1-\exp\left(\frac{\Delta v}{c_e}\right)\right]\left[\frac{1}{1+(c_e/\Delta v)^2(\Delta v/kv_A)^2}-1\right]-\frac{1}{2}\right\} \times\left[\left(\frac{c_e}{\Delta v}\right)^2+\left(\frac{kv_A}{\Delta v}\right)^2\right] \tag{9}$$

Equation (9) shows that the normalized flight time τ_I^* is only a function of $\Delta v/c_e$ and $kv_A/\Delta v$ and can, therefore, be integrated into Fig. 4.

Figure 4 shows the field of all possible optimal values for a certain mission in the case of an ion, a Hall ion, an MPD propulsion, or a high-power thermal arcjet system in the form of a nomograph. With a given thruster type, that is, with a given kv_A and $\eta_{T,\max}$, a given power supply with α_{PS} and η_{PC}, and a given mission, that is, Δv, the optimal exhaust velocity c_e and the minimal flight time τ can be determined for a certain payload fraction, for example.

Thermal Arcjet Thrusters

In addition to the case of high-power thermal devices that have already been discussed in the preceding section, the degree of ionization and also the fraction of the thermal losses of a thermal arcjet change by varying the effective exhaust velocity c_e. Therefore, Eq. (5) cannot be used. However, for thermal arcjets, the effective exhaust velocity c_e is a linear function of the specific power $P_{\mathrm{el}}/\dot{m}$ over a wide range of operation. Therefore, in this case the assumption can be made that

$$c_e = a + b(P_{\mathrm{el}}/\dot{m}) \tag{10}$$

Parameter a represents an exit velocity that corresponds to the energy content of the propellant that is not directly influenced by the arc. In the case of a thruster that is not regeneratively cooled, a corresponds to the cold-gas thrust and, therefore, increases as the size of the thruster and the power level increase. With an increasing regenerative capacity of the thrusters, which is the highest for the MARC 6 (Medium Power Arcjet 6), and with an increasing heat capacity of the propellant, a also increases (Table 3).

Parameter b represents the slope of the curves in Fig. 5. On the one hand, it depends on the propellants being highest for hydrogen, which offers high exit velocities even at low specific power levels. This can be seen in curves 1–3. In the case of NH_3 or N_2H_4, the curves are steeper due to dissociation. For these two propellants, b differs only slightly because it is very close to the Alfvén velocity; b generally increases with increasing Alfvén velocity and decreasing molecular weight because c_e strongly depends on the effective molecular weight. On the other hand, an increase of the regenerative cooling capacity makes b smaller, which is obvious from the very low value of the Marc 6.

For the thrust efficiencies, when Eq. (10) is used,

$$\eta_T = T^2/2\dot{m}P_{\mathrm{el}} = c_e^2/(2P_{\mathrm{el}}/\dot{m}) = (b/2)\left[c_e^2/(c_e-a)\right] \tag{11}$$

follows.

Table 3 Various thermal arcjet thrusters[a]

Thruster	Propellant	a, km/s	b, s/km	Experimentally verified c_e area, km/s	Experimentally verified P_{el} area, W	Ref.
ATOS-2	NH_3	2.75	$6.74E-02$	4.3–5.6	900–1,600	24
ARTUS	N_2H_4	2.49	$6.60E-02$	4.2–5.2	1,000–1,600	25
ARTUR	H_2	4.46	$4.00E-02$	7.2–9.3	1,000–1,800	24
Marc6	H_2	7.97	$2.09E-02$	10.2–12.2	5,000–9,150	24
HIPARC	H_2	4.44	$2.97E-02$	8–12	24,000–39,000	4
NASA	N_2H_4	4.74	$2.60E-02$	6–7.1	1,000–2,500	26

[a]With Eq. (10) in the case of HIPARC only the data for medium power operation (<39 kW) is included.

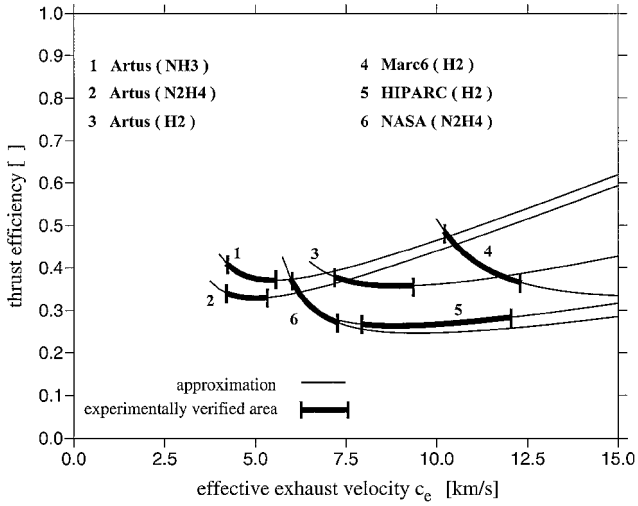

Fig. 6 Thrust efficiency η_T as function of effective exhaust velocity for different thermal arcjet thrusters and propellants (Table 3).

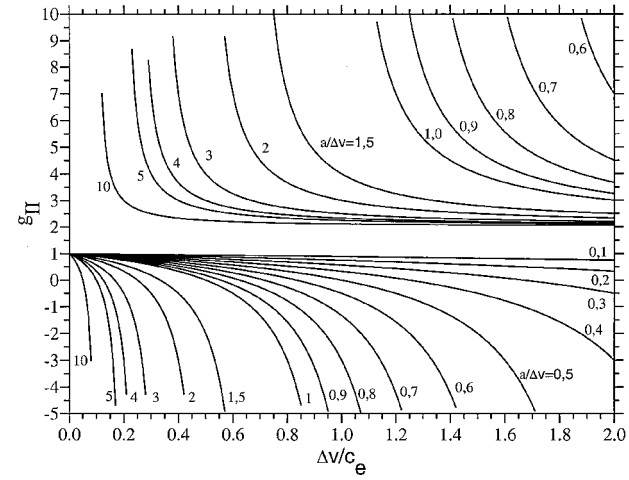

Fig. 7 Function of g_{II} vs $\Delta v/c_e$ with the mission and propulsion system dependent parameter $a/\Delta v$.

In Fig. 5 the effective exhaust velocity c_e of different arcjets listed in Table 3 is plotted against the specific power. Figure 5 makes it clear that the effective exhaust velocity increases as the thruster size increases due to an increase of specific power. The High Power Arcjet (HIPARC) thruster is optimal for high-power levels (100 kW). Only for the low-power level of this thruster can it be handled with Eq. (10). For high-power operation, Eq. (5) has to be applied; this is included in the preceding section. The thrusters have not been optimized for the power levels shown in this section.

Figure 6 shows the thrust efficiencies calculated for thermal arcjet propulsion systems. The experimentally verified area is plotted with a thick line; the thin line represents the curves that are obtained using Eqs. (10) and (11). The assumption of linearity matches the experimental results very well except for the very low and very high c_e region for a specific thruster. The very low values are not of any technical interest. At very high c_e values, that c_e no longer increases as the specific power rises in a linear manner is a sign that the gas is nearly fully dissociated. In addition, the fraction of ionization is no longer increasing at the same rate as in the lower c_e area. For high-power thermal arcjets, the point can even be reached where, as with MPD thrusters, the gas is nearly fully ionized and the degree of ionization no longer changes by increasing c_e. In this case, the behavior of the device can be handled using Eq. (5).

When Eq. (11) is introduced into the left-hand side of the optimization condition in Eq. (4), the function $g_{II}\,(a, c_e)$ can be obtained, which is valid for thermal arcjets in the boundaries discussed earlier,

$$g_{II} = \frac{c_e - 2a}{c_e - a} = \frac{1 - 2(a/\Delta v)(\Delta v/c_e)}{1 - (a/\Delta v)(\Delta v/c_e)} \tag{12}$$

Plotted against $\Delta v/c_e$ with the propulsion system and mission-dependent parameter $a/\Delta v$, one obtains the set of curves given in Fig. 7.

As in the case of the function f, no g_{II} values exist between 1 and 2. The function g_{II} becomes singular for $\Delta v/c_e = \Delta v/a$ or $c_e = a$. This point is not of importance; only the region of $c_e > a$ is of interest because a corresponds to the effective cold-gas thrust. Therefore, the upper part of Fig. 7 for $g_{II} \geq 2$ is not of interest, and one can concentrate on the region f, $g_{II} \leq 1$. In the upper part of the nomograph, the functions f and g_{II} are plotted with the payload and structure mass fraction μ_{LS}, or rather $a/\Delta v$, as parameters. It can be seen from Fig. 7 that for a specific mission, that is, $\Delta v = \text{const}$, the required optimal exhaust velocity $c_{e,\text{opt}}$, to even be able to conduct an optimization, increases with a and, therefore, with the thruster size.

As in the case of the thruster types in the preceding section, a normalized trip time τ^*_{II} can also be derived for thermal arcjet thrusters from the optimization condition (4) with respect to Eq. (12) using the rocket equation (2) to eliminate the payload and structure fraction μ_{LS},

$$\tau^*_{II} = \frac{c_e}{\Delta v}\left[\frac{\exp(\Delta v/c_e) - 1}{\Delta v/c_e} + \frac{a}{\Delta v}\frac{\Delta v}{c_e} - 1\right] \tag{13}$$

with the normalized trip time defined as

$$\tau^*_{II} = \eta_{PC}\alpha_{PS}(b/\Delta v)\tau \tag{14}$$

From Eq. (13), it follows that the normalized trip time is only a function of $a/\Delta v$ and $\Delta v/c_e$ and could, therefore, be integrated into the nomograph in Fig. 8. This nomograph describes the field of all possible optimal values for a certain mission in the case of a thermal arcjet propulsion system. With a given propulsion system, that is, with given values a, b, α_{PS}, and η_{PC} for a specific mission, that is, Δv, the optimal exhaust velocity $c_{e,\text{opt}}$ and the minimal flight time $\tau_{\min}$ can be determined, for example, for a certain payload fraction.

Optimization of a Transport Rate

Not only are the performance data of the propulsion system and the reliability important for missions, but ultimately the costs play a decisive role. An attempt will be made to model these costs with a relatively simply defined transport rate and to include this transport rate in the mission optimization.

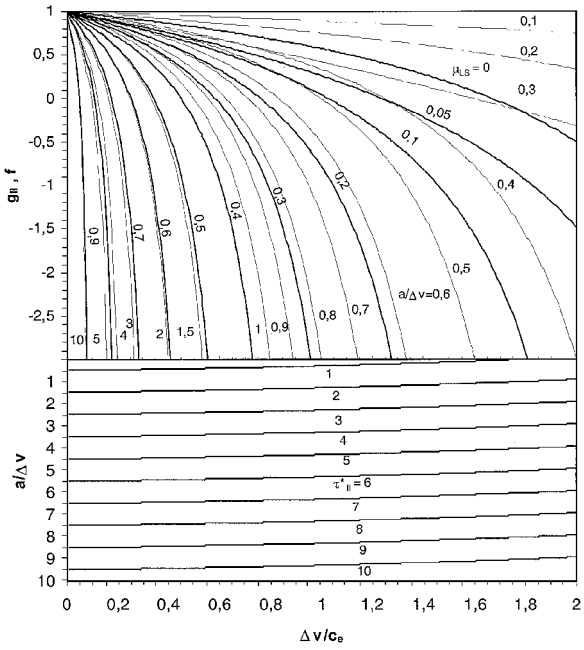

Fig. 8 Nomograph of the quantities Δv, τ^*, μ_{LS}, and c_e for the optimized rocket equation for thermal arcjet thrusters.

If the payload and structure mass m_{LS} are related to the total propulsion mass at the onset of the mission (propulsion system mass m_{PS} plus propellant mass m_P) multiplied by the flight time τ, one obtains the following definition of a transport rate (TR):

$$\mathrm{TR} = m_{LS}/(m_{\mathrm{PS}} + m_P)\tau \tag{15}$$

When Eq. (3) is used, the TR can be expressed as

$$\mathrm{TR} = \mu_{LS}/(1 - \mu_{LS})\tau \tag{16}$$

which means that TR is only a function of the flight time τ and the payload and structure mass fraction μ_{LS}. Substituting τ in Eq. (16) with the rocket equation (2) provides TR as a function of μ_{LS}, c_e, and Δv:

$$\mathrm{TR} = \frac{2\alpha_F \mu_{LS}[\mu_{LS}\exp(\Delta v/c_e) - 1]}{c_e^2(1 - \mu_{LS})[1 - \exp(\Delta v/c_e)]} \tag{17}$$

Therefore, the necessary conditions for a maximal TR for a specific mission Δv are that the partial differentiations with respect to c_e and μ_{LS} be zero. Because the TR is only dependent on c_e over $\tau(c_e)$, the condition $\partial \mathrm{TR}/\partial c_e$ is satisfied if $\partial\tau/\partial c_e = 0$. The resulting equation was deduced in an earlier section in the rocket equation optimization as Eq. (4). Because the specific power α_F is not a function of the payload fraction μ_{LS}, the condition $\partial \mathrm{TR}/\partial \mu_{LS} = 0$ yields the following simple equation for the payload mass fraction μ_{LS}:

$$\mu_{LS} = 1 - \sqrt{1 - \exp(-\Delta v/c_e)} \tag{18}$$

For a given mission and propulsion system, the specific power α_F and the velocity increment Δv are fixed, and the TR only depends on the exhaust velocity c_e and payload and structure mass fraction μ_{LS}. An investigation of the second derivative shows the maximum TR when both conditions are satisfied. Substituting Eq. (18) into Eq. (4) provides

$$\underbrace{\frac{c_e}{\alpha_F}\frac{\partial \alpha_F}{\partial c_e}}_{g} = 2$$

$$- \underbrace{\frac{(\Delta v/c_e)\exp(\Delta v/c_e)\sqrt{1 - \exp(-\Delta v/c_e)}}{[1 - \exp(\Delta v/c_e)]\left[\left(1 - \sqrt{1 - \exp(-\Delta v/c_e)}\right)\exp(\Delta v/c_e) - 1\right]}}_{f_{\mathrm{TR}}} \tag{19}$$

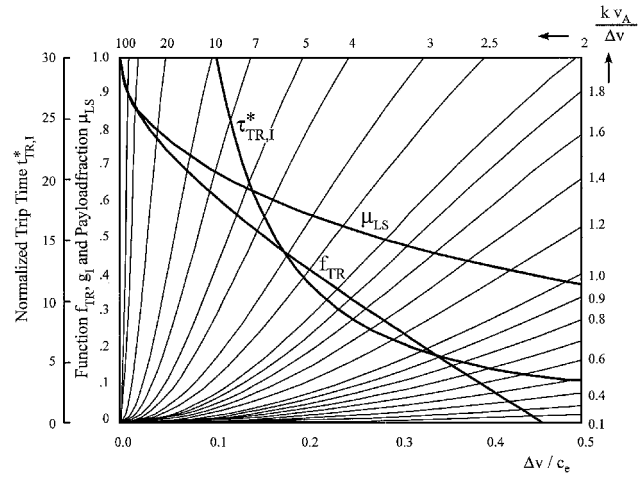

Fig. 9 Diagram of Δv, c_e, μ_{LS}, and $\tau^*_{\mathrm{TR},I}$ for high power thermal arcjets, ion, Hall ion, and MPD thrusters for the case of an optimized transport rate.

With the additional Eq. (18), the function $f = f_{\mathrm{TR}}$ has become dependent only on $\Delta v/c_e$ and is no longer dependent on the mass fraction μ_{LS}, as in the case of the optimization of the rocket equation.

High-Power Thermal Arcjets, Ion, Hall Ion, and MPD Thrusters

It has been shown in the preceding section that for high-power thermal arcjets as well as for ion, Hall ion and MPD thrusters the function g becomes g_I [see Eq. (7)]. The function $f_{\mathrm{TR}}(\Delta v/c_e)$ can now be plotted together with $g_I(\Delta v/c_e)$, with $kv_A/\Delta v$ as parameter that, in contrast to $f(\Delta v/c_e, \mu_{LS})$, no longer represents a set of curves (shown later). Thus, for a given propulsion system and mission, the intersection of f_{TR} with g_I $(\Delta v/c_e, kV_A/\Delta v)$ yields one solution for an optimal specific impulse. In accord with Eq. (18), the function $\mu_{LS}(\Delta v/c_e)$ was also plotted in Fig. 9, so that one immediately obtains the corresponding payload mass fraction value μ_{LS}. Also in Fig. 9, the normalized flight time $\tau^*_{\mathrm{TR},I}(\Delta v/c_e)$ is shown. The normalized flight time has been calculated with the use of Eqs. (1), (2), (7), (8), (18), and (19) as

$$\tau^*_{\mathrm{TR},I} = (c_e/\Delta v)^3[\exp(\Delta v/c_e - 1)]\sqrt{1 - \exp(\Delta v/c_e)} \tag{20}$$

For a given mission Δv and a given propulsion system (kv_A, $\eta_{T,\max}$, α_{PS}, and η_{PC}), the exhaust velocity c_e, the payload and structure mass fraction μ_{LS}, and the flight time τ can be determined from Fig. 9 and Eq. (8) so that the TR is optimal.

Thermal Arcjet Thrusters

In the case of a thermal arcjet thruster, the function g becomes g_{II} [see Eq. (12)], which is plotted in a set of curves $g_{II}(\Delta v/c_e)$ in Fig. 7 with $a/\Delta v$ as parameter. In the same way as for the thrusters, dealt with in the preceding section, the functions $f_{\mathrm{TR}}(\Delta v/c_e)$ [Eq. (19)], μ_{LS} [Eq. (18)], and $\tau^*_{\mathrm{TR},II}$ can be integrated in one graph. This is shown in Fig. 10.

The normalized flight time $\tau^*_{\mathrm{TR},II}$ can be calculated from the optimization condition (18), substituting μ_{LS} with the help of the rocket equation (2) and using, in addition, the optimization condition (19) and Eqs. (12) and (14):

$$\tau^*_{\mathrm{TR},II} = \frac{[\exp(\Delta v/c_e) - 1]\left[\left(1 - \sqrt{1 - \exp(-\Delta v/c_e)}\right)\exp(\Delta v/c_e) - 1\right]}{(\Delta v/c_e)^2\exp(\Delta v/c_e)\left[\sqrt{1 - \exp(-\Delta v/c_e)} - 1\right]} \tag{21}$$

For a given mission Δv and a given thermal arcjet propulsion system (a, b, α_{PS}, and η_{PC}), the exhaust velocity c_e, the payload and structure mass fraction μ_{LS}, and the flight time τ can be determined from Fig. 10 and Eq. (14) so that the TR is optimal.

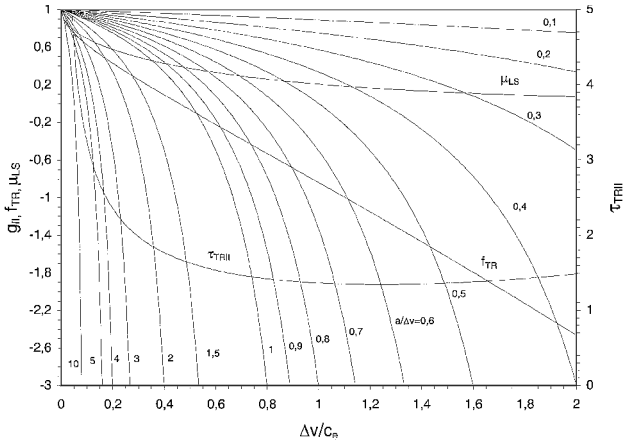

Fig. 10 Diagram of Δv, c_e, μ_{LS}, and $\tau^*_{TR,II}$ for thermal arcjet thrusters for the case of an optimized TR.

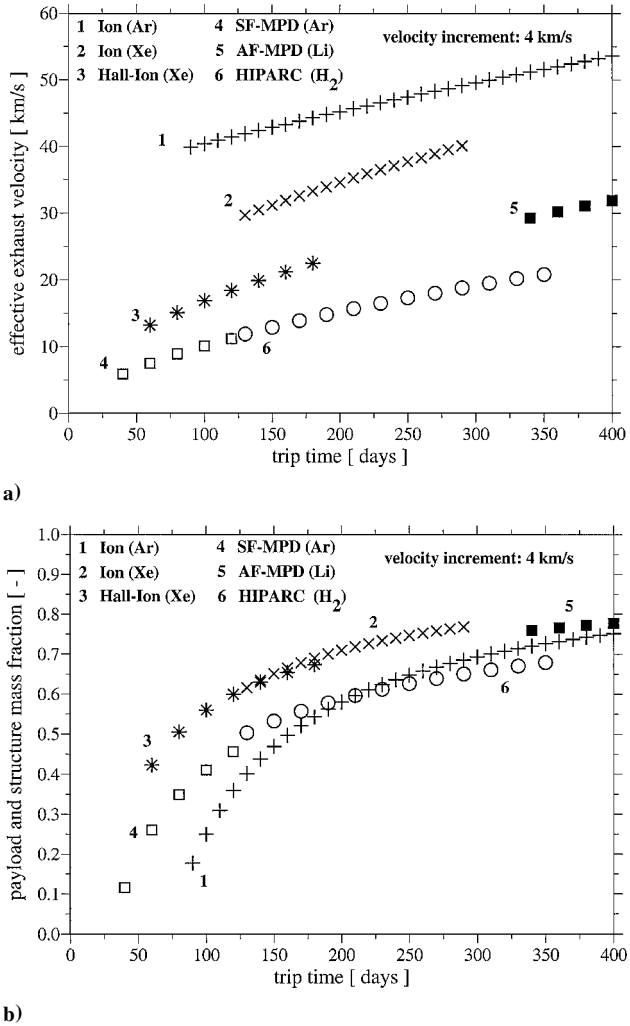

Fig. 11 For thrusters in Table 2 for a velocity increment of Δv = 4 km/s: a) effective exhaust velocity c_e and b) payload and structure mass fraction μ_{LS} vs flight time τ.

Comparison of Results for Different Thruster Types

In this section, the results of the different optimizations are compared for selected thruster types listed in Tables 2 (see Refs. 4, 5, and 20–23) and 3 (see Refs. 4 and 24–26). The corresponding efficiencies are shown in Figs. 3 and 6. As power supply, a nuclear reactor such as the SP-100 (Ref. 27) was selected with a specific power of $\alpha_{PS} = 33$ W/kg. This reactor was chosen with regard to interplanetary missions. To allow for a better comparison, the same α_{PS} was also used as the basis for the thermal arcjet thrusters. This corresponds to a mean value for solar power supplies. For all thrusters, the efficiency of the power conditioner was chosen with $\eta_{PC} = 0.9$.

Optimized Rocket Equation

The results for the high-power thermal arcjets, ion, Hall ion, and MPD thrusters (Table 2) are shown. The optimized exhaust velocities c_e and the payload and structure mass fractions μ_{LS} for two velocity increments, $\Delta v = 4$ and 9 km/s, as a function of the flight time, are shown in Figs. 11 and 12.

The optimal exhaust velocities c_e decrease as the flight time τ decreases (Figs. 11a and 12a). Furthermore, they decrease slightly as the velocity increment Δv increases. It is obvious that the optimal exhaust velocity not only depends strongly on the thruster type but also on the propellant. The difference between argon (number 1) and xenon (number 2) with the same ion thruster is more than 10 km/s (Figs. 11 and 12). It shows that the optimal exhaust velocities c_e depend not only on the maximum attainable thruster efficiency $\eta_{T,\max}$ but also on the factor $k v_A$ in Eq. (5), which is a sort of loss factor. The highest values result for the argon ion thruster (number 1) and the lowest for the self-field (SF) MPD thruster (number 4) and the high-power thermal arcjet (number 6), also with argon as the propellant. Both follow the same curve. However, so far, the exhaust velocities of the SF-MPD thruster have only achieved the optimal value for low trip times. For long trip times, an improvement of the c_e is required. In contrast, the high-power thermal arcjet thruster shows optimal effective exhaust velocities for long trip times. The required optimal exhaust velocities are clearly higher for the applied-field (AF)

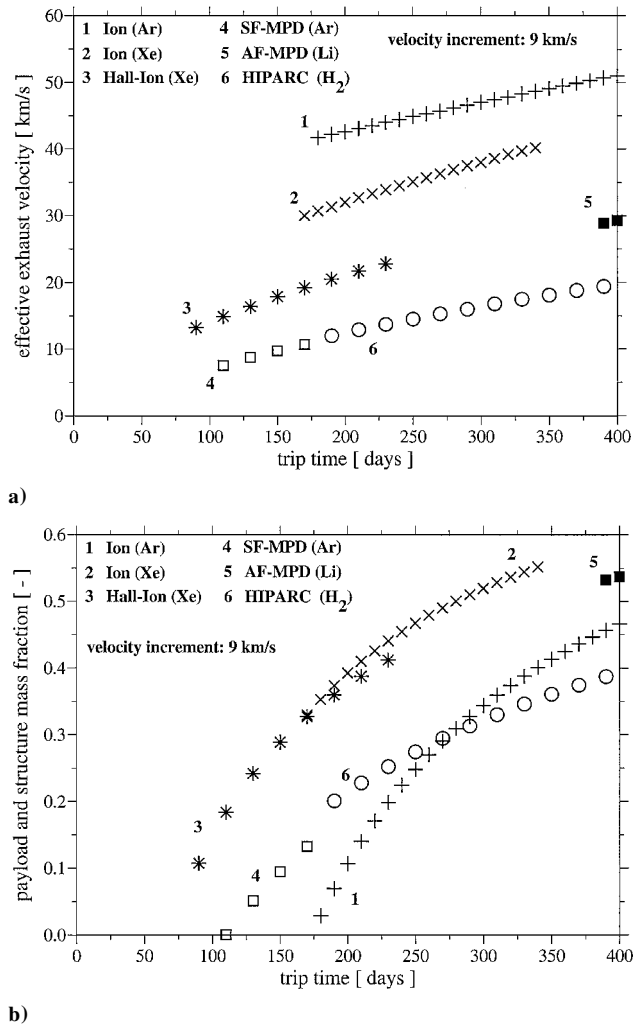

Fig. 12 For thrusters in Table 2 for a velocity increment of Δv = 9 km/s: a) effective exhaust velocity c_e and b) payload and structure mass fraction μ_{LS} vs flight time τ.

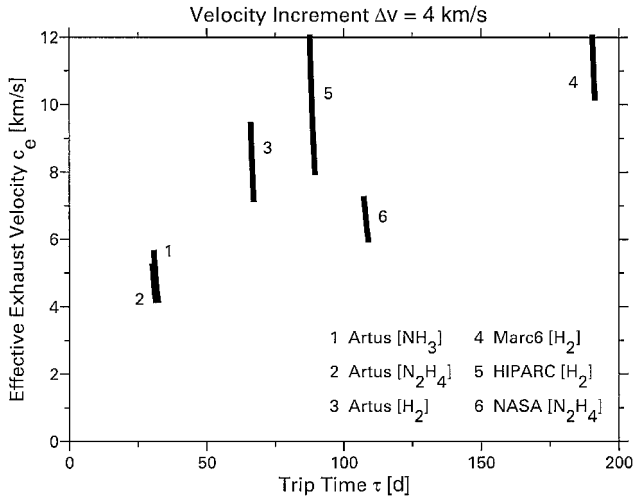

a)

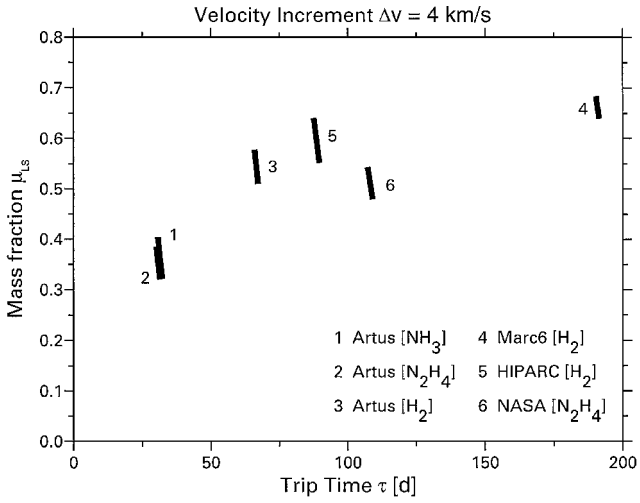

b)

Fig. 13 For thrusters in Table 3 for a velocity increment of Δv = 4 km/s: a) effective exhaust velocity c_e and b) payload and structure mass fraction μ_{LS} vs flight time τ.

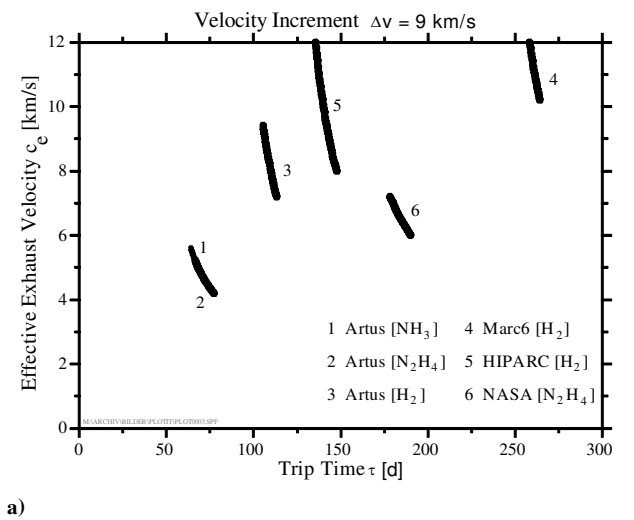

a)

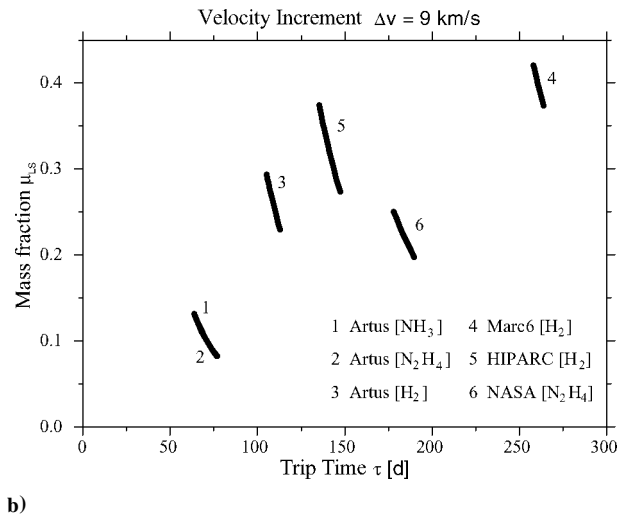

b)

Fig. 14 For various thrusters in (Table 3) for a velocity increment of Δv = 9 km/s: a) effective exhaust velocity c_e and b) payload and structure mass fraction μ_{LS} vs flight time τ.

MPD thruster (number 5) with lithium compared to the SF device and are even higher for the Hall ion thruster (number 3), but clearly lower compared to the ion thruster with the same propellant (Xe). It is evident that optimal exhaust velocities with an AF-MPD thruster with lithium as propellant can only be achieved for low-velocity increments Δv, and very long trip times. Over a wide range of missions the c_e values attainable with this device are much too high. In comparison, with the Hall ion thruster, the effective exhaust velocity is high enough only for short trip times. As far as optimal exhaust velocities c_e are concerned, the thruster types are very distinct with the exceptions of the SF-MPD and the high-power thermal arcjet. This is not the case for the maximal payload and structure mass fraction μ_{LS}. The xenon ion and Hall ion thrusters both attain the best payload fraction because of their superior $\eta_{T,\max}$ in the region of operation, the Hall ion thruster for the short trip times, and the Xe ion thruster for the long trip times. For the thermal arcjets (Table 3), the results for the same velocity increment (4 and 9 km/s) are shown in Figs. 13 and 14.

It is apparent in Figs. 13 and 14 that, for a specific Δv requirement, for every thruster an optimal exhaust velocity can be only given within a small flight time area. This flight time area shifts for a specific thruster with increasing Δv toward longer flight times. It can also be shown that the optimal effective exhaust velocity increases as the Δv requirement increases.[28] Note that because of the flat τ_{II}^* curves, uncertainties in determining parameter a have a strong influence on $c_{e\,\mathrm{opt}}$ (Fig. 8).

Optimization for a TR

The results for the optimization of the TR for the six selected thrusters in Table 2 are shown in Fig. 15 as a function of the velocity increment Δv. The picture of the results compared to those of the optimization of the rocket equation has changed completely: The optimal exhaust velocities c_e increase as the Δv rises (Fig. 15a) and asymptotically approach the optimization boundary, which is determined by the intersection of the f_1 curve with the abscissa in Fig. 9. The minimal exhaust velocities given by the optimization procedure and that would be attained at $\Delta v = 0$ are equal to the kv_A values from Eq. (5).

This can be explained with Fig. 9. $\Delta v = 0$ also means that $\Delta v/c_e = 0$, and therefore, g_I must be equal to 1. For $g_I = 1$, Eq. (7) can only be achieved with an exhaust velocity equal to kv_A. The experimentally verified regions where an optimization is possible are indicated with thick lines in Figs. 15a–15d. For the AF-MPD thruster, the optimal effective exhaust velocities considered here with the whole Δv region are far below the values that can be achieved with this lithium thruster.[28]

From Fig. 15a it is evident, for example, that the Hall ion thruster SPT-100 only offers optimal effective exhaust velocities for velocity increments between 2.2 and 8 km/s. If higher and lower Δv values are required, the optimal exhaust velocities cannot be achieved because they are too low for low Δv and too high in the case of high Δv. Therefore, if one wants to use this thruster for a low Δv mission (<2.2 km/s), the lowest possible c_e should be used; in the case of a high Δv mission (>8 km/s), the highest c_e would be the best

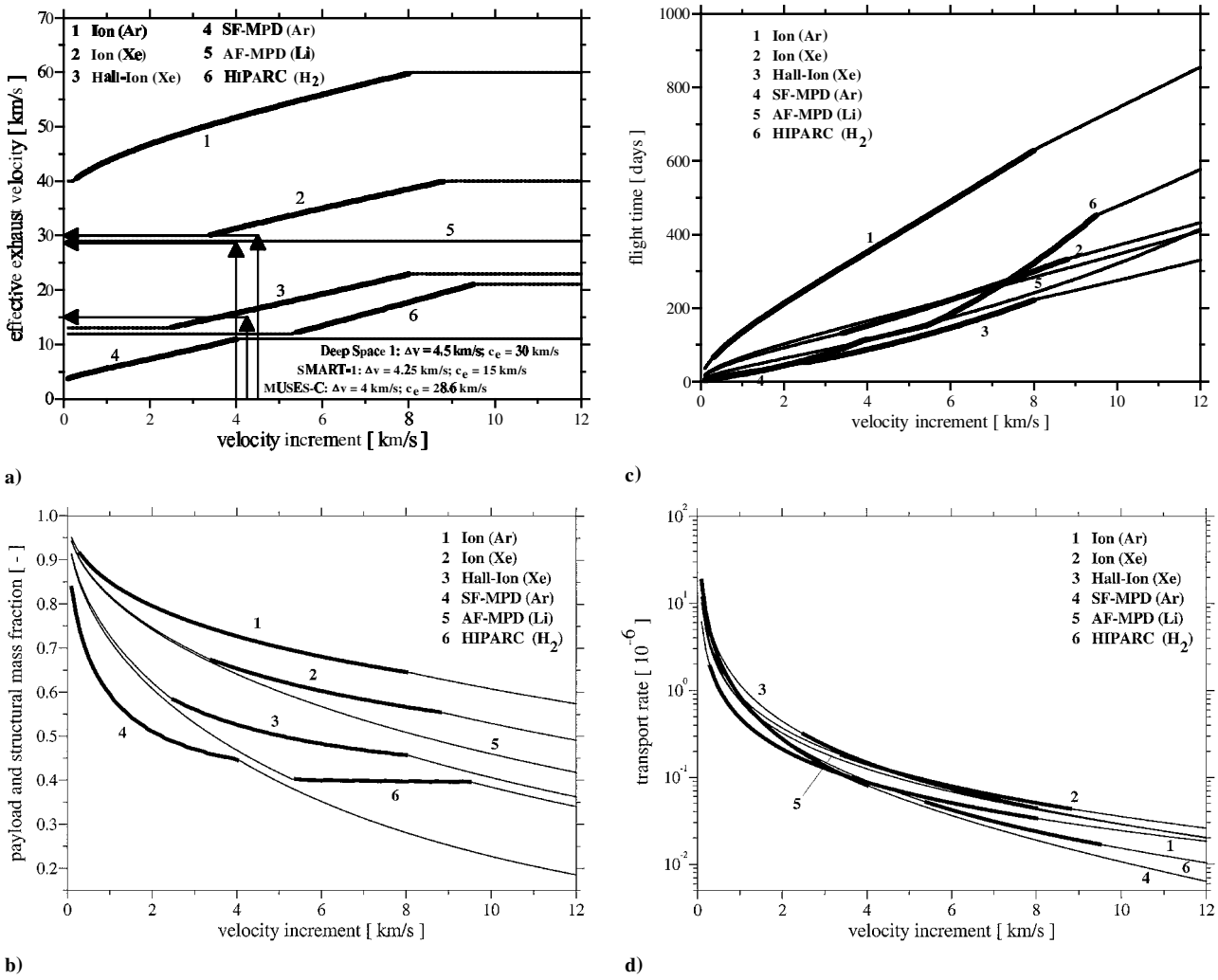

Fig. 15 For thrusters in Table 2: a) effective exhaust velocity c_e, b) payload and structure mass fraction μ_{LS}, c) flight time τ, and d) TR vs velocity increments for the TR optimization.

choice. These considerations lead to the thin lines in Fig. 15a. For the regions with a constant effective exhaust velocity, the transport rate only depends on μ_{LS}. Therefore, Eq. (18) represents the only optimization condition and can be used for calculating μ_{LS} (thin lines in Fig. 15b). The corresponding flight time in this case can be calculated from the rocket equation (2) and leads to the thin lines in Fig. 15c.

Also, the curves for the payload and structure mass fraction μ_{LS} (Fig. 15b) show behavior different from those of the preceding rocket equation optimization (Figs. 11 and 12). The μ_{LS} values for the optimized region fall steadily from 1 to an asymptotic value determined by the maximal ratio of $\Delta v/c_e$ [Fig. 9 and Eq. (18)]. The best payload fractions are achieved for the argon ion thruster (number 1) due to its very high exit velocities, the worst for the self-field MPD thruster (number 4) and the high power thermal arcjet (number 6) (Fig. 15). The corresponding mission flight times τ, plotted in Fig. 15c, show quite a changed character. The lowest trip times can be achieved by using the SF-MPD thruster (number 4) for low-velocity increments up to 2.2 km/s and the Hall ion thruster for high Δv.

The optimization rate is defined so that it is large when a short flight time, as well as a large payload fraction, is achieved. Figure 15d makes it clear that, for velocity increments up to 3.5 km/s, the Hall ion thruster offers the highest transport rate due to its low loss factor. At velocity increments higher than 6 km/s, the xenon ion thruster clearly takes over this good position due to its very high-efficiency value. The SF-MPD thruster, which in contrast to the Hall ion thrusters and ion thrusters has not yet been optimized, is so far only preferable for very low-velocity increments.

For three recent missions, Deep Space 1 (ion thruster, Xe), SMART-1 (Hall ion thruster, Xe) and Muses-C (ion thruster, Xe), the effective exit velocities of each chosen thruster are included in Fig. 15a. The effective exhaust velocities agree quite well with the chosen operating points for the missions despite the simple TR model. Note that the ion thrusters for both missions do not completely agree with thruster 2. Because the thrust efficiency dependence on exit velocity is not available or accessible to us for these devices, the correct calculation could not be performed.

The results for the optimization of the TR for the six selected thermal arcjet thrusters in Table 3 are shown in Fig. 16. The experimentally verified regions where an optimization is possible are plotted as a thick line. Figure 10 has already shown that the optimal effective exhaust velocity for a specific Δv requirement now only depends on the parameter $a/\Delta v$. The same is true in view of Eq. (18) for μ_{LS}. In other words, the larger a is, the faster the exit velocity that corresponds to the energy content of the propellant that is not directly influenced by the arc, the larger the c_e required for an optimization and the larger the μ_{LS}. This means that improving the regenerative cooling capacity results in an increase of the payload and structure mass fraction. Figure 16a shows how the optimal exhaust velocity decreases as the velocity increment increases within the optimization region. An optimization of the Marc 6 thruster with small velocity increments, for example, is not possible because the optimal c_e can no longer be achieved. This means that for a small velocity increment, the largest possible c_e should be chosen. If, on the other hand, one wants to use a thruster for a mission with a larger Δv requirement than its optimization area covers, it should

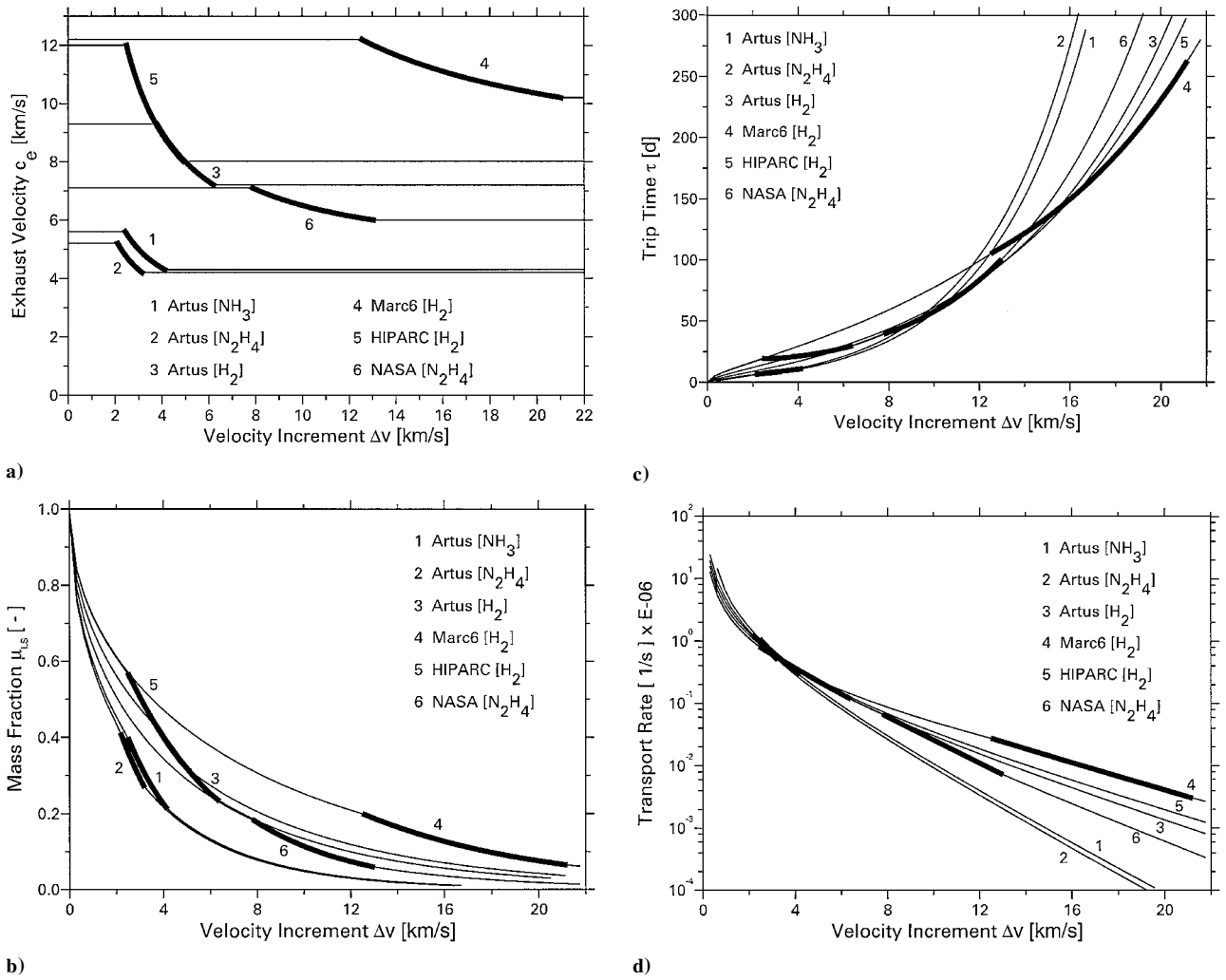

Fig. 16 For thrusters in Table 3: a) effective exhaust velocity c_e, b) payload and structure mass fraction μ_{LS}, c) flight time τ, and d) TR vs velocity increment for the extended TR optimization.

be operated with the smallest possible c_e because then the higher efficiency (Fig. 6) increases the transport rate. These considerations led to the results indicated by thin lines in Fig. 16a. For the regions with a constant effective exhaust velocity, the transport rate depends only on μ_{LS}. Therefore, Eq. (18) represents the only optimization condition and can be used for the calculation of μ_{LS} (thin lines in Fig. 16b). The corresponding flight time in this case can be calculated from the rocket equation (2) and leads to the results shown by thin lines in Fig. 16c. Generally speaking, the transport rate sinks as the velocity increment increases because the flight time (Fig. 16c) as well as the payload and structure mass fraction (Fig. 16b) sink drastically. This behavior is visible in Fig. 16d. Figure 16 shows that the smaller and likewise optimized thruster Artus is superior when the Δv requirement is small (<3 km/s). For $\Delta v > 6$ km/s, the Marc 6 is superior due to its good regenerative cooling capacity. At this performance level, HIPARC can only be included in the comparison to a limited extent because it has only a relatively low regenerative cooling capacity, in which respect its stage of development and that of the thrusters Artus and Marc are not equivalent.

In Fig. 17 the transport rates of only four of the thrusters (two from each of the two groups discussed) are compared. Although the exhaust velocity that the Marc 6 exhibits in the Δv region investigated is too low (compare Fig. 16a), its transport rate is superior to all of the other thrusters when the entire region is considered. This is due to the significantly shorter flight times that can be achieved. Here the large potential of the thermal arcjets is obvious.

Through its optimal exhaust velocity, the high-power arcjet HIPARC has already distinguished itself in the Δv region that is of interest for many missions. If it is possible to increase signifi-

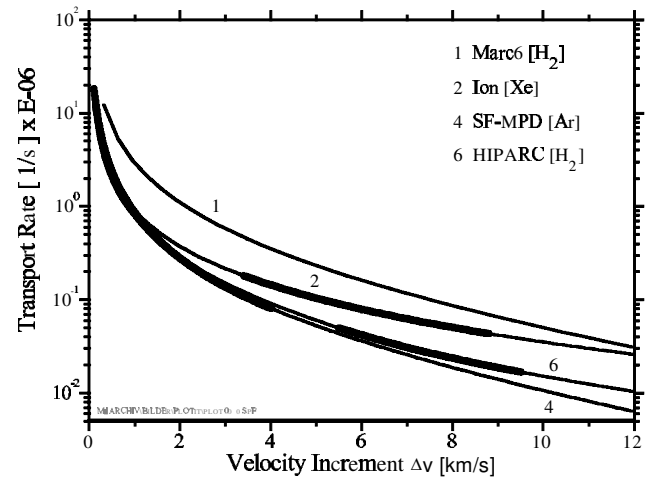

Fig. 17 TR as a function of velocity increment (kilometers per second) for selected thrusters.

cantly HIPARC's efficiency through regenerative cooling and optimization, it will be of great interest for transfer and interplanetary missions.

Despite the high payload ratio that can be achieved with these thrusters, the Xe ion thruster's TR is significantly lower than that of the Marc 6 because the flight time is very long due to the low-thrust density that these thrusters exhibit. Significant improvements are no longer possible for these devices. For SF-MPD thrusters, it is valid

to say that their efficiency as well as their effective exhaust velocity must be improved to make these devices competitive.

Conclusions

The purpose of this paper is to include the dependency of the specific power α_F on the exhaust velocity c_e the flight mission parameter optimization and to show the tendencies of the results, not to give detailed solutions, for which the mass fraction division, for example, would not be sufficiently refined. The results clearly show the strengths and weaknesses of individual thrusters and the influence of the propellant choice. When the individual thrusters are compared, note that the thrusters are in various stages of development. In some cases, there are already optimized and qualified thrusters (for example, the Xe ion thruster, Hall ion thruster, low-power arcjet, and Marc 6). On the other hand, the regenerative cooling capacity of the HIPARC, for example, is far from exhausted, and there are only simple laboratory models of the MPD thrusters.

In the case of the AF-MPD thruster, lithium is certainly not the best propellant choice because the effective exhaust velocity is too high. If the exhaust velocity could be lowered, the TR would improve.[28] Certain important aspects in choosing the optimal thruster are not included in the optimization, such as the attainable thrust density lifetime, reliability, and possible contamination. Despite numerous simplifications, it could be shown for a number of current mission examples that the optimal effective exhaust velocities could be predicted fairly well.

Acknowledgments

We thank Thomas Wegmann and Jörg Heiermann for their help with the figures.

References

[1]Sovey, J., Rawlin, V., and Patterson, M., "Ion Propulsion Development Projects in U.S.: Space Electric Rocket Test I to Deep Space I," *Journal of Propulsion and Power*, Vol. 17, No. 3, pp. 517–526.

[2]Saccoccia, G., "European Activites in Electric Propulsion," *Proceedings of the 3rd International Conference on Spacecraft Propulsion*, ESA Publications Div., Noordwijk, The Netherlands, 2000, pp. 49–63.

[3]Toki, K., Kuninaka, H., Funaki, I., Nishiyama, K., and Shimizu, Y., "Development Status of a Microwave Ion Engine System for the Muses-C Mission," *Proceedings of the 26th International Electric Propulsion Conference*, Japan Society for Aeronautical and Space Sciences, Tokyo, 1999, pp. 753–760.

[4]Auweter-Kurtz, M., Gölz, T., Habiger, H., Hammer, F., Kurtz, H., Riehle, M., and Sleziona, C., "High Power Hydrogen Arcjet Thrusters," *Journal of Propulsion and Power*, Vol. 14, No. 5, 1998, pp. 764–773.

[5]Wegmann, T., Auweter-Kurtz, M., Habiger, H., Kurtz, H., and Schrade, H. O., "Experimental Comparison of Steady State Nozzle Type and Cylindrical MPD Thrusters at High Current Levels," *Proceedings of the 23rd International Electric Propulsion Conference*, Electric Rocket Propulsion Society, Fairview Park, OH, 1993, pp. 1124–1133.

[6]Rehder, J. J., and Wurster, K. E., "Electric vs Chemical Propulsion for a Large Cargo Orbital Transfer Vehicle," *Journal of Spacecraft and Rockets*, Vol. 16, No. 1, 1974, p. 129.

[7]Kaufmann, H. R., and Robinson, R. J., "Electric Thruster Performance for Orbit-Raising and Maneuvering, *Orbit-Raising and Maneuvering Propulsion-Research Status and Needs*, edited by L. H. Caveny, Vol. 89, Progress in Astronautics and Aeronautics, AIAA, New York, 1984, pp. 303–326.

[8]Jones, R. M., "Comparison of Potential Electric Propulsion Systems for Orbit Transfer," *Journal of Spacecraft and Rockets*, Vol. 21, No. 1, 1984, pp. 88–95.

[9]Regetz, J. D., and Terwilleger, L. H., "Cost Effective Technology Advancement Directions for Electric Propulsion Transportation Systems," *Electric Propulsion and its Applications for Space Missions*, edited by R. C. Finke, Vol. 79, Progress in Astronautics and Aeronautics, AIAA, New York, 1981, pp. 82–98.

[10]Masek, T. D., and Ward, J. W., "Economics of Ion Propulsion for Large Space Systems," AIAA Paper 78-698, April 1978.

[11]Silva, T. H., and Byers, D. C., "Nuclear Electric Propulsion System Utilization for Earth Orbit Transfer of Large Spacecraft Structures," AIAA Paper 80-1223, June 1980.

[12]Langmuir, D. B., "Low Thrust Flight: Constant Exhaust Velocity in Field-Free Space," *Space Technology*, edited by H. S. Seifert, Wiley, New York, 1959, pp. 9-01–9-22.

[13]Irving, J. H., "Low Thrust Flight: Variable Exhaust Velocity in Gravitational Fields," *Space Technology*, edited by H. S. Seifert, Wiley, New York, 1959.

[14]Stuhlinger, E., *Ion Propulsion for Space Flights*, McGraw–Hill, New York, 1964, pp. 10-01–10-54.

[15]Vondra, R. J., and Caveny, L. H., "Plasma Thruster Research in the U.S.A.," *Proceedings of the 17th International Electric Propulsion Conference*, Japan Society for Aeronautical and Space Sciences, Tokyo, 1984, pp. 20–27.

[16]Auweter-Kurtz, M., Kurtz, H. L., and Schrade, H. O., "Optimization of Electric Propulsion Systems Considering Specific Power as Function of Specific Impulse," *Journal of Propulsion and Power*, Vol. 4, No. 6, 1988, pp. 512–519.

[17]Kim, V., Garkusha, V., Murashko, V., Popov, G., and Tikhonov, V., "Modern Trends of Electric Propulsion Activity in Russia," *Proceedings of the 26th International Electric Propulsion Conference*, Japan Society for Aeronautical and Space Sciences, Tokyo, 1999, pp. 27–32.

[18]Auweter-Kurtz, M., *Lichtbogenantriebe für Weltraumaufgaben*, B. G. Teubner, Stuttgart, Germany 1992, pp. 17–19.

[19]Bühler, R. D., "Plasma Thruster Development: Magnetoplasmadynamic Propulsion, Status and Basic Problems," U.S. Air Force Rocket Propulsion Lab., Rept. AFRPL TR-86-013, Edwards AFB, CA, Sept. 1986.

[20]Rawlin, V. K., "Operating of the y-Series Thruster Using Inert Gas," AIAA Paper 82-1929, June 1982.

[21]Arhipov, B. A., Krochak, L. Z., Kudriavcev, S. S., Murashko, V. M., and Randolph, T., "Investigation of the Stationary Plasma Thruster (SPT-100) Characteristics and Thermal Maps at the Raised Discharge Power," AIAA Paper 98-3791, July 1998.

[22]Tikhonov, V., Semenikhin, S., Brophy, J. R., and Polk, J. E., "The Experimental Performances of the 100 kW Li MPD Thruster with an External Magnetic Field," *Proceedings of the 24th International Electric Propulsion Conference*, The U.S. Air Force European Office of Aerospace Research and Development, London, 1995, pp. 718–724.

[23]Tikhonov, V., Semenikhin, S., Brophy, J. R., and Polk, J. E., "Performance of 130 kW MPD Thruster with an External Magnetic Field and Li as a Propellant," *Proceedings of the 25th International Electric Propulsion Conference*, Electric Rocket Propulsion Society, Fairview Park, OH, 1997, pp. 728–733.

[24]Riehle, M., Laux, T., Huber, F., Kurtz, H. L., and Auweter-Kurtz, M., "Performance Evaluation of Regeneratively Cooled 1, 10 & 100 kW Arcjets," *Proceedings of the 26th International Electric Propulsion Conference*," Japan Society for Aeronautical and Space Sciences, Tokyo, 1999, pp. 176–185.

[25]Riehle, M., "Entwicklung eines 1 kW Hydrazin Triebwerkes–Bericht der IRS Aktivitäten," Final Presentation, DARA Fkz 50-TT-9401, Inst. of Space Systems, Universität Stuttgart, March 1998.

[26]Curran, F. M., and Byers, D. C., "New Developments and Research Findings: NASA Hydrazine Arcjets," AIAA Paper 94-2463, June 1994.

[27]Buden, D., and Garrison, P. W., "Design of a Nuclear Electric Propulsion Orbital Transfer Vehicle," *Journal of Propulsion*, Vol. 1, No. 1, 1985, pp. 70–76.

[28]Auweter-Kurtz, M., "Optimization of Electric Thrusters for Primary Propulsion," AIAA Paper 2001-3347, July 2001.